Chapter 2
Group 1-Group 2 Bimetallic Alkyls and Hydrides

2.1 Introduction

Main group heterobimetallic compounds are extremely common and encompass a variety of simple salts and cluster types. The interactions that dominate the coordination chemistry of the s-block metals in particular have yielded a huge variety of heterobimetallic complexes. These generally contain elements of the alkali- and alkaline earth-metals, or both, bridged by alkoxide, amide or halide ligands [1, 2].

The extension of this motif to more reactive carbanion and hydride ligands however is less common. Carbanion containing mixed Group 1-Group 2 heterobimetallics are dominated by metallocycle anion bridges, with a far more limited number of alkyl-, and aryl-terminated species reported, as shown in Scheme 2.1 [3, 4].

The structures of the early main group metal hydrides are dominated by saline species of the form MH_n (Group 1; n = 1, Group 2; n = 2) [5] wherein ionic or bridging structures yield extended networks. Recently, however, a variety of molecular Group 2 hydrides have been structurally characterised, spurred on by investigations into the postulated intermediacy of these species in a variety of H–C [6], Si–N [7], Si–O [8] and B–N [9] bond forming reactions. The lighter congeners of the saline s-block hydrides have, in spite of their structure, been identified as potential hydrogen storage materials as a result of their relatively high hydrogen weight percentages (LiH; 12.7 % [10], MgH_2; 7.6 % [11]). Utilisation of these species in this application is, however, hindered by their large lattice energies relative to the bulk metals, which require impractically high hydrogen release temperatures (LiH; 858 kJ mol^{-1}, MgH_2; 2791 kJ mol^{-1}). Recent calculations regarding magnesium hydride have suggested a reduction in cluster size of $(MgH_2)_n$ (n < 19) can lower these temperatures [12]. As a result, a variety of higher magnesium hydride clusters have been synthesised utilising a molecular approach; generally relying upon the reaction of organometallic complexes bearing reactive metal bound substituents with phenylsilane. The Hill group reported the first hydride-rich magnesium cluster, $[(IPr)_2Mg_4H_6\{N(SiMe_3)_2\}_2]$ (IPr = ((HCN{2,6-*i*$Pr_2C_6H_3$})$_2$C:) (**IX**) supported by bulky amides and N-heterocyclic carbene ligands with a magnesium to hydride ratio of 1:1.5 (Scheme 2.2) [13].

D.J. Liptrot, *Group 2 Mediated Dehydrocoupling*, Springer Theses,
DOI 10.1007/978-3-319-21036-0_2

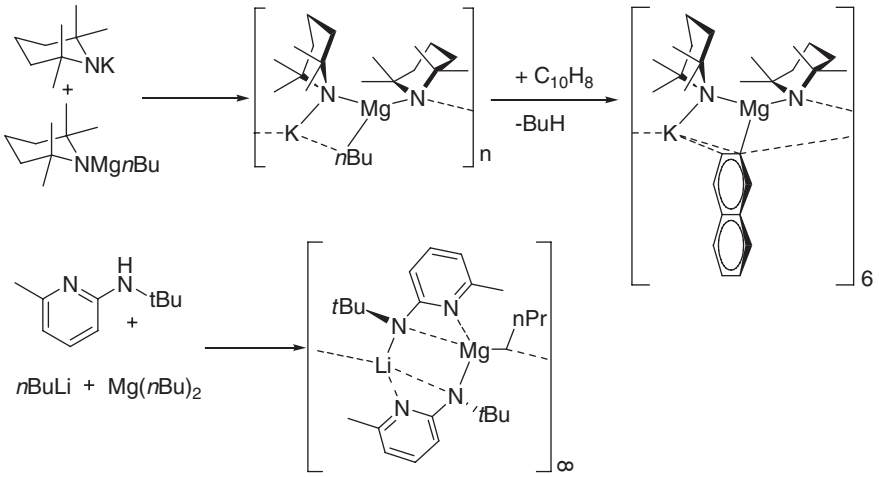

Scheme 2.1 Previously reported synthetic routes and crystallographically defined structures of heterobimetallic s-block clusters with alkyl or aryl substituents

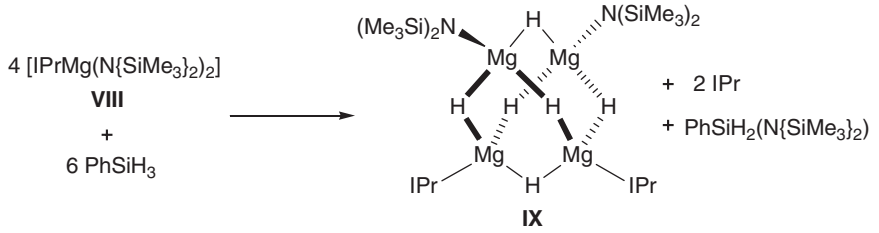

Scheme 2.2 The synthetic route reliant upon σ-bond metathesis utilised by the Hill group to yield their record-breaking magnesium hydride cluster, IX

Subsequent work from the group of Harder has shown the utility of β-diketiminate ligands in the formation of higher magnesium hydrides yielding [(PARA)$_3$Mg$_8$H$_{10}$] (PARA = 1,4-C$_6$H$_4${2,6-*i*Pr$_2$C$_6$H$_3$NC(Me)C(H)C(Me)N}$_2$) [14] and [{NN-(MgH)$_2$}$_2$] (NN = {2,6-*i*Pr$_2$C$_6$H$_3$NC(Me)C(H)C(Me)N}$_2$) [15].

In contrast to this burgeoning body of work in Group 2 metal hydrides, structurally characterised molecular hydrides of Group 1 have proved more elusive (Fig. 2.1). Alongside the remarkable "superaggregate" [(*t*BuOLi)$_{16}$(LiH)$_{17}$] [16], generated photolytically, only a relatively small number of molecular Group 1 hydrides have been synthesised by the rational application of a silane derivative to a reactive metal precursor. These are the bulky phosphinoamide (**XI**) and pyrazolate supported clusters described by Stasch [17, 18]. Instead, prior work in the field of Group 1 hydrides has been dominated by mixed metal "ate" structures, most notably the 'inverse crowns' [M$_2$Mg$_2$(N*i*-Pr$_2$)$_4$(μ-H)$_2$·(toluene)$_2$] (M = Na (**Xa**), K (**Xc**)) [19, 20] reported by Mulvey and co-workers which are thought

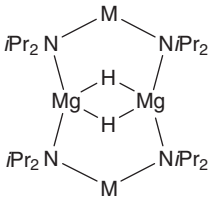

Xa: M = Na(C_7H_8); **Xb**: Na; **Xc**: K(C_7H_8)

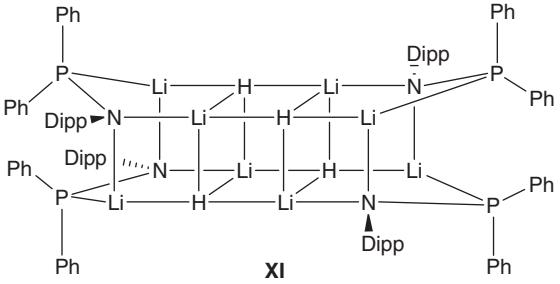

Fig. 2.1 The crystallographically defined structures of a heterobimetallic and homometallic s-block hydride cluster

Scheme 2.3 The proposed synthetic route to **Xa**-**c** via a β-hydride elimination

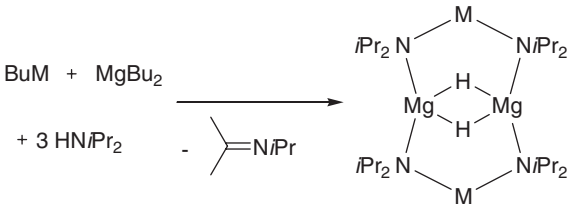

to form via a serendipitous β-hydride elimination from the N*i*-Pr_2 ligands of the bimetallic trisamides [M(μ-N*i*Pr_2)$_2$Mg(N*i*Pr_2)], synthesized in situ, as shown in Scheme 2.3 [20].

2.2 s-Block Mixed Metal Amidoalkyls

Extensive work by Mulvey and co-workers has demonstrated the enhanced reactivity of heterobimetallic s-block amides of the form [M(μ_2-NR_2)$_2$M′(NR_2)] (M = Group 1 metal; M′ = Group 2 metal) in a variety of contexts [1]. Seeking to capitalise on this foundation, an alternative synthetic approach to heterobimetallic hydrides may be envisaged based on mixed s-block amidoalkyls of the form [M{N($SiMe_3$)$_2$}$_2$MgBu], [M = Li (**1**), Na (**2**), K (**3**)]. The bulky hexamethyldisilazide ligand was selected for both its relevance in catalysis and its steric characteristics while the reactive alkyl group is anticipated to allow selective reactivity with phenylsilane.

Compounds **1**-**3** were readily synthesised at room temperature via the 1:1 reaction of [BuMg{N($SiMe_3$)$_2$}], synthesised in situ by the reaction of an equimolar mixture of di-butylmagnesium and hexamethyldisilazane, and subsequent addition of the relevant [M{N($SiMe_3$)$_2$}] complex in toluene (Scheme 2.4). Crystallisation from the reaction mixture at −34 °C yielded the desired compounds suitable for single crystal X-ray diffraction analysis.

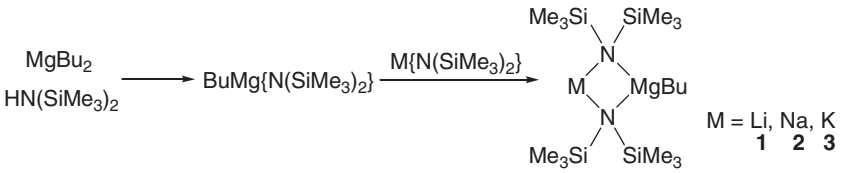

Scheme 2.4 The synthetic approach to heterobimetallic s-block amidoalkyls utilised in this work yielding **1**–**3** (M = Li, Na, K respectively)

Table 2.1 The unit cell parameters for complexes **1**–**3**

	1	**2**	**3**
a/Å	9.2930(1)	9.3020(2)	9.2520(2)
b/Å	20.3790(4)	20.6500(4)	20.5140(4)
c/Å	13.8580(3)	13.9670(3)	14.6960(3)
α/°	90	90	90
β/°	98.2550(10)	96.493(1)	93.112(1)
γ/°	90	90	90

Compounds **1**–**3**, when isolated under similar conditions crystallise in the $P2_1/n$ space group and show only a very limited variation in unit cell dimensions. A slightly greater variation in β (Table 2.1) is however indicative of notable variations in the deduced crystal structures.

Compound **1** appears to crystallise as a 88:12 mixture of isomers (**1**:**1′**); the major fraction being that indicated in Scheme 2.4 (**1**), while the minor fraction consists of the isomer wherein the magnesium and lithium ions have exchanged places (**1′**). Given the similarity in the ionic radii of Li^+ and Mg^{2+}, the solution stability of BuLi and the propensity of s-block metals to undergo Schlenk-type equilibria, this disorder is unsurprising. Furthermore, although extensive debate still exists as to the degree of covalency in lithium organometallics calculations have indicated that such covalency is accessible [21]. This is similar to magnesium wherein Mg–C bonds have a significant degree of covalency but contrasts with the heavier alkali metals wherein M–C bonds are entirely ionic. In contrast, both **2** and **3** crystallise with magnesium solely in the 3-coordinate position, while the alkali metal displays a 2-coordinate geometry; a potential reflection of the distinct ionic radii of the cations and the insolubility of the relevant MBu compounds. In the case of **3**, the asymmetric unit was disordered 50:50 with regards to its orientation, and furthermore an evident undetermined systematic issue with the data was apparent from the high residuals after refinement (R1 = 0.1637 *wR*2 = 0.4190). The connectivity, however, was unambiguous and, while the bond length and angle data must be treated with caution, a number of structural trends are evident. The crystallographically defined structures of these species are shown in Figs. 2.2, 2.3 and 2.4 and relevant bond length and angle data shown in Table 2.2. During the course of the preparation of this thesis, compound **2** was independently described by O'Hara and co-workers. Crystallographic data for both compounds

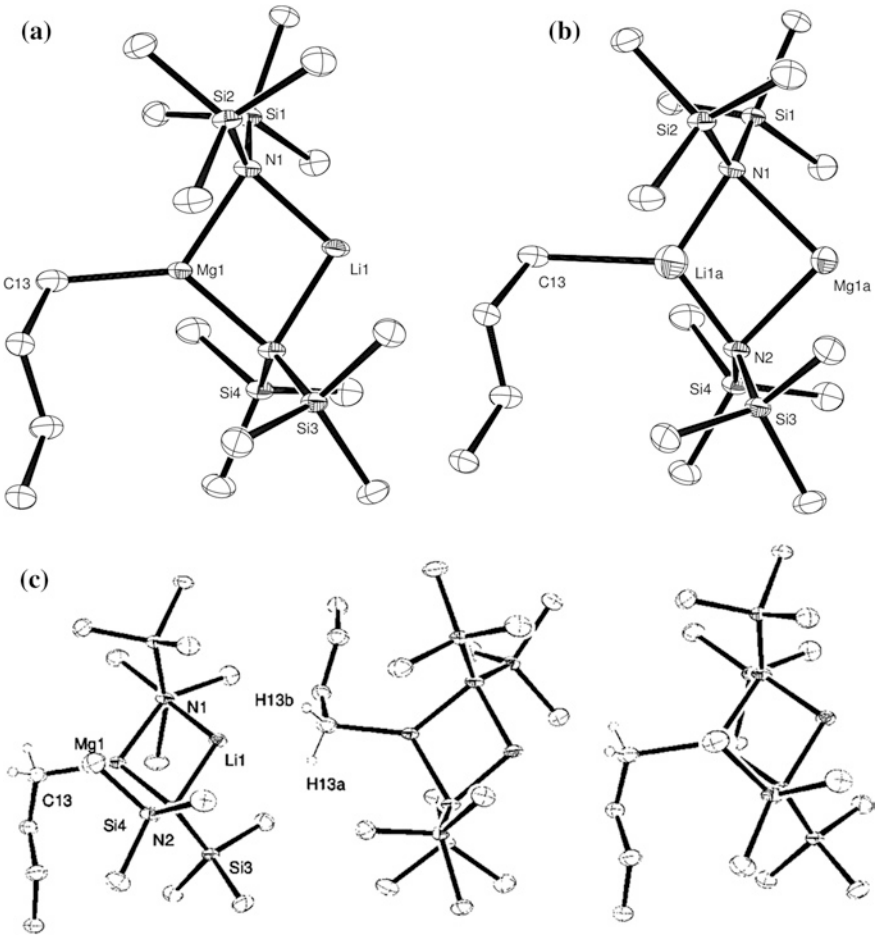

Fig. 2.2 **a** ORTEP representation of **1**, ellipsoids set to 30 %, hydrogen atoms omitted for clarity. **b** ORTEP representation of **1′**, ellipsoids set to 30 %, hydrogen atoms omitted for clarity. **c** ORTEP representation of the repeating unit of **1** in the solid state, ellipsoids set to 30 %, hydrogen atoms except those attached to C13 omitted for clarity

are identical however all analysis and data contained herein was independently collected for this thesis [22].

As shown in Figs. 2.2, 2.3 and 2.4, the isostructural complexes **1**-**3** crystallise as linear arrays with alternating orientations of the *n*-butyl chains, in a manner reminiscent of the amidopyridine-alkyl species reported by Kays and coworkers [4]. The authors note therein the novelty of the observed bridging butyl groups wherein an Mg-C···Li contact is observable. In contrast, no significant interaction between the independent molecules in **1** is readily observable. This can likely be attributed to the far larger hexamethyldisilazide ligands in contrast to the

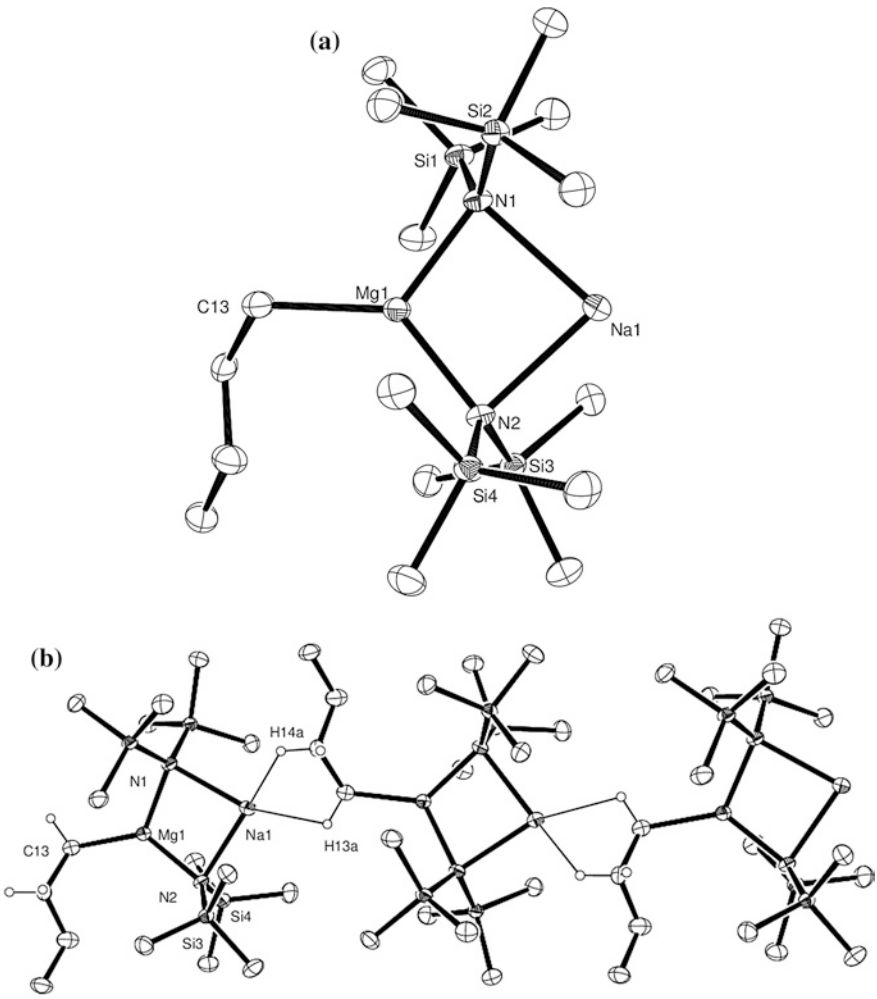

Fig. 2.3 **a** ORTEP representation of **2**, ellipsoids set to 30 %, hydrogen atoms omitted for clarity. **b** ORTEP representation of the repeating unit of **2** in the solid state, ellipsoids set to 30 %, hydrogen atoms except those attached to C13 and C14 omitted for clarity

amidopyridines in this previous report. In contrast, however, both **2** and **3** show significant intermolecular interactions as a result of the increased alkali metal cation size. In contrast to the interactions observed by Kays and co-workers, however these are not of the form Mg-C···M but instead appear to comprise Mg-CH···M and Mg-C(H)$_2$-CH···M contacts to yield a solid state polymer bound by anagostic interactions. As noted, no significant H···Li contact is discernible in **1**, while in **2** and **3** the H···M contact is evident. Two notable variations between **2** and **3** can be further observed. **2** shows a significant anagostic interaction with not only H13a,

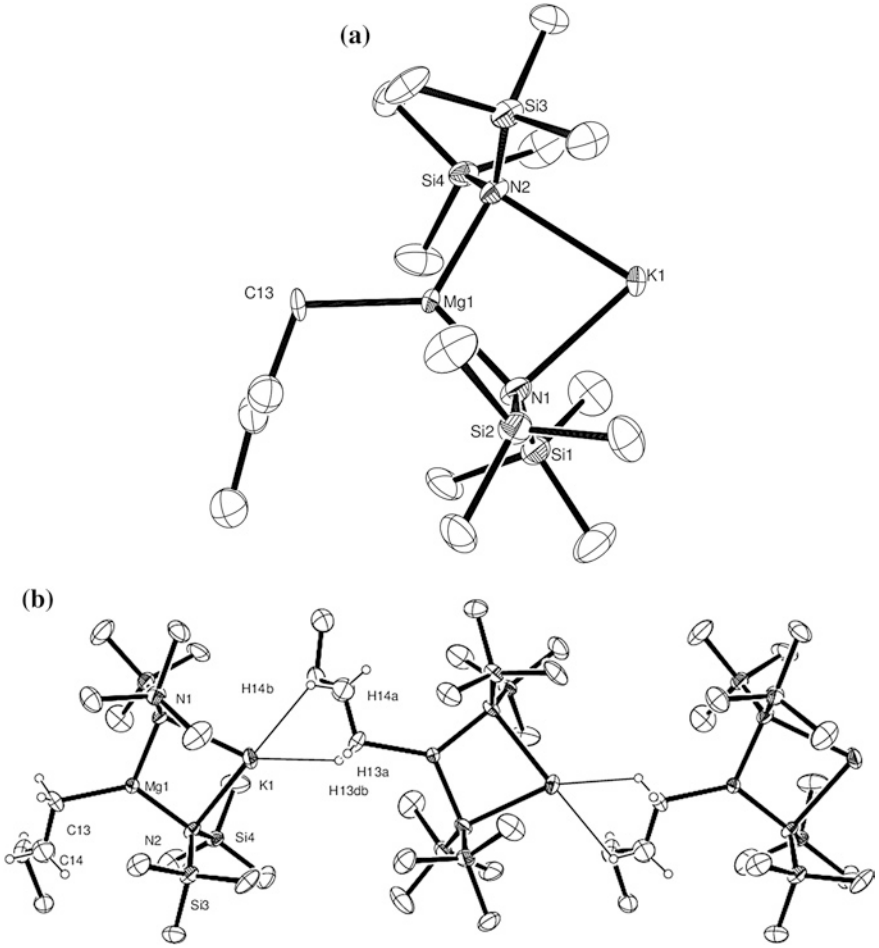

Fig. 2.4 **a** ORTEP representation of **3**, ellipsoids set to 30 %, hydrogen atoms omitted for clarity. **b** ORTEP representation of the repeating unit of **2** in the solid state, ellipsoids set to 30 %, hydrogen atoms except those attached to C13 and C14 omitted for clarity

projecting from the α-methylene of the *n*-butyl chain but also H14a which projects from the β-methylene. This second interaction, although also present in **3** appears to be significantly weaker. In contrast, the H13a···K interaction in **3** appears to be stronger than the corresponding interaction for its lighter congener, **2**, as reflected in the elongation of the H13a···M interaction being less than the change in ionic radius from Na^+ to K^+.

These interactions appear to have significant structural consequences, with Mg1-C13 bond of **2** being shorter than that of **1** while both are exceeded by the analogous measurement in **3**. Correspondingly, an increase in the Mg-C13-C14

Table 2.2 Selected bond lengths and bond angles for **1**–**3**

	1	**2**	**3**
M1-N1	2.054(18)	2.466(2)	2.767(9)
M1-N2	2.073(16)	2.436(2)	2.755(9)
Mg1-N1	2.097(3)	2.095(2)	2.175(10)
Mg1-N2	2.089(3)	2.0798(1)	2.118(9)
Mg1-C13	2.181(4)	2.152(3)	2.19(2)
H13a-M1′	2.165	2.443	2.532
H14a-M1′	2.572	2.213	2.705
M1-N1-Mg1	81.6(5)	84.34(7)	87.8(3)
M1-N2-Mg1	81.3(5)	85.43(7)	89.2(3)
N1-M1-N2	99.4(8)	85.03(7)	76.5(2)
N1-Mg1-N2	97.49(13)	105.05(8)	105.5(4)
N1-Mg1-C13	127.95(14)	124.44(9)	123.0(7)
N2-Mg1-C13	134.51(13)	130.44(9)	131.2(7)
Mg1-C13-C14	112.9(2)	114.90(17)	114.2(17)

angles of **2** and **3** in contrast to **1**, is observed which could be attributed to the decrease in the N(1,2)-Mg-C13 angles. Given the clear interactions within the unit cell and the limited change between **2** and **3**, however, as well as the influence of H14a-Na interactions in **2**, it is more likely that this angle is rendered more obtuse by the interactions between the butyl chain and the Group 1 cation of a neighbouring molecule.

Although these data may be affected by both the poor quality of the crystallographic data for **3** and the constraints utilised to separate the modelling of the isomers in **1**, it is notable that this trend of **1** may be consistently differentiated from **2** and **3** for other means of analysis as well as the crystallography (vide infra). It is thus suggested that these observed variations can be attributed to the species occupying two classes—those which have significant anagostic interactions (**2** and **3**) and those which do not (complex **1**). This observation can be used to rationalise the subsequent structural and spectroscopic variations seen for complexes **1**-**3**, as well as the existence of an alternate, crystallographically defined isomer **1′**, wherein the lack of stabilising anagostic interactions reduce the drive towards the major isomer, **1**.

In all three complexes the magnesium centre remains trigonal planar with the angles around Mg adding up to ~360°. However, unsurprisingly, the move from the smaller Li to the larger K cation via the intermediate Na leads to an elongation in the M–N bond. Notably, the increase in M–N bond length from **1** to **2** is significantly larger than the variation in the ionic radius of lithium versus sodium. This is not, however, true of the increase in bond length from **2** to **3** which is of a similar magnitude to the ionic radii. This increase in bond length occurs concurrently with an increase in the M-N-Mg angle and a corresponding decrease in the N-M-N angle, with the increasingly acute angles at the Group 1 centre leading to an increasing planarization of the MgN_2M fragment. Consequently the N-Li-N plane in **1** sits 5.26° from the N-Mg-N plane, while **2** is closer at 4.52° and **3** is

Table 2.3 Selected NMR spectroscopic data (ppm) for compounds **1**–**3**

	1	**2**	**3**
M-C$\underline{H}_2$ $\delta 1_H$	0.01	−0.07	−0.40
M-$\underline{C}H_2$ $\delta 13_C$	11.2	12.1	14.0
$N(SiMe_3)_2$ $\delta 1_H$	0.17	0.19	0.22
$N(SiMe_3)_2$ $\delta 13_C$	5.1	6.0	6.3
$N(SiMe_3)_2$ $\delta 15_N$	47.3	47.0	49.7

closer still at 2.63°, possibly a reflection of the increased coordinative flexibility of the alkali metals down Group 1 or as a result of increasing potential for the formation of anagostic interactions. Also notable is the effect of the increasing Group 1 cation size on the geometry of the magnesium centre, with the N-Mg-N angle being forced to be increasingly obtuse by the increasingly dominant size of the Group 1 centre.

Although these solid-state structural parameters noted hint to the effects of the variation in alkali metal upon complexes **1**-**3**, the ^{1}H, ^{13}C and ^{15}N NMR data, as summarised in Table 2.3, provide clearer electronic discrimination.

The aforementioned elongation of the N–M bond lengths between Li and K leads to a corresponding deshielding of the silylmethyl carbon centre and protons present on the hexamethyldisilazide ligand. The trend in the ^{15}N NMR spectroscopic shifts is more complex, however, suggesting that increasing N-M length does not simply yield a deshielding of the nitrogen nucleus. This increase in shielding between **1** to **2** but significant decrease from **2** to **3** appears to mirror the trends observed for the M-N and Mg-C bond lengths and indicate a significant structural shift from **1** to **2** followed by a less profound variation from **2** to **3**. However, the unreferenced nature of the ^{15}N NMR spectroscopy performed here renders these conclusions tentative at best.

Perhaps of most significance is the variation in the ^{13}C and ^{1}H NMR spectroscopic chemical shifts for the α-methylene of the butyl chain. In contrast to the observed variation in Mg-C bond length, a smooth progression in deshielding of the ^{13}C NMR resonance attributed to C13 from **1** to **3** is observed, suggesting an interplay of stereoelectronic factors. The α-methylene ^{1}H NMR signal once again provided a smooth progression in chemical shift; perversely however this occurred as an increased shielding of these protons from **1** to **3**. This counterintuitive trend could be a simple reflection of the paramagnetic contribution to the ^{13}C NMR chemical shifts, it could also be a direct result of the persistence of intermolecular interactions occurring in solution in a similar manner to those observed in the solid state for **2** and **3**. Further evidence for the persistence of interactions of this form can be provided by analysing the effect of concentration upon the ^{1}H NMR shift of the α-CH_2 protons which shows almost no concentration dependence for **1** but a small dependence for **2** and **3**. The increasing shielding of the α-CH_2 protons versus deshielding of the carbon centre is thus a reflection of a balance between the Mg-C13 and H13···M bond strengths in which the latter interaction is increasingly augmented at the expense of the former as the size of the Group 1 cation increases.

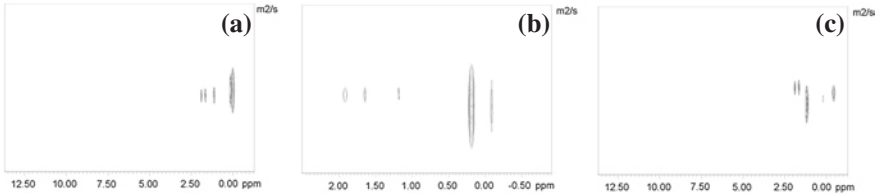

Diffusion coefficient of proton/ m s^{-2}		**2**	**3**
$C\underline{H}_3$	$8.95x10^{-10}$	$8.42x10^{-10}$	$7.67x10^{-10}$
$C\underline{H}_2$	$9.01x10^{-10}$	$8.38x10^{-10}$	$7.41x10^{-10}$
$C\underline{H}_2$	$8.93x10^{-10}$	$8.22x10^{-10}$	$7.41x10^{-10}$
Mg-$C\underline{H}_2$	$8.88x10^{-10}$	$8.69x10^{-10}$	$7.46x10^{-10}$
$(N(Si\underline{Me}_3)_2)$	$8.81x10^{-10}$	$8.68x10^{-10}$	$7.61x10^{-10}$

Fig. 2.5 The DOSY spectra and diffusion coefficients for compounds **1**–**3**

To further probe the possibility of solution intermolecular interactions, these species were subjected to DOSY analysis as summarised in Fig. 2.5.

As shown, visual inspection of the DOSY parameters suggested each compound retained its solid state structure in solution, with the hexamethyldisilazide and *n*-butyl resonances all sharing very similar diffusion coefficients.

Complexes **1** and **3** were further subjected to variable temperature NMR experiments which showed these species to be stable up to 95 °C. This stability contrasts with the previously observed reactivity for di-*iso*-propylamide-ligated structures **Xa-c** (vide supra).

Previously reported mixed metal clusters bound by hexamethyldisilazide ligands, such as $[\{(Me_3Si)_2N\}Ca\{\mu\text{-}N(SiMe_3)_2\}_2Mg\{N(SiMe_3)_2\}]$ as well as the parent $[Mg\{N(SiMe_3)_2\}_2]$ show extensive solution fluxionality reflecting the Schlenk-like equilibria to which these species are prone [2]. Indeed, in the former case ^{1}H NMR analysis reflects the presence of all possible hexamethyldisilazide-bound Group 2 complexes comprising of either the homoleptic Mg and Ca diamide species, as well as the bimetallic species in solution. Gratifyingly, in the case of **1**-**3** the major peaks observable in ^{1}H NMR spectrum could be attributed to compounds possessed of a solution structure corresponding to that observed in the solid state as defined by crystallography. Notable, however, were the presence of minor peaks in the region characteristic of hexamethyldisilazide silylmethyl resonances observed in the ^{1}H NMR spectra of **1**-**3** which would appear to indicate some solution equilibria occurring faster than the NMR timescale. Although minor peaks tentatively attributed to the butyl resonances of alternative solution isomers were also identifiable, these could not be rationally integrated and matched to any of the observed silylmethyl resonances. The extreme relative intensity of the hexamethyldisilazide peak corresponding to the crystallographically defined structures of **1**-**3** may be responsible for masking the corresponding resonances, thus complicating this analysis. Notably, the observed disorder in the crystallographically

defined structure of **1/1′** and reactivity of **2** with donor molecules observed by O'Hara and co-workers were also liable to be reflections of these equilibration processes (vide supra).

2.3 s-Block Mixed Metal Hydrides

Although β-hydride elimination has previously yielded bimetallic s-block hydrides supported by amide ligands, approaches towards these species utilising σ-bond metathesis have remained hitherto unreported. This contrasts with the common routes to both homometallic Group 1 and Group 2 species which have predominantly relied upon the activity of hydridic silanes with relevant metal amides or alkyls. It was thus speculated that σ-bond metathesis with silanes would take place selectively with the relatively unbulky and reactive alkyl groups borne by **1**–**3** could yield a variety of novel heterobimetallic hydrides structurally related to **Xa**-**c**. Furthermore, these reactions were investigated for the relevance of such a step to dehydrocoupling, particularly of silanes and amines.

To assess this possibility, solutions of **1**–**3** were reacted with equimolar quantities of phenylsilane in d_8-toluene on an NMR scale. The ^{1}H NMR spectrum resulting from the reaction of compound **3** under these conditions suggested the formation of $PhSi(H)_2n$-Bu and three broad, metal-bound hexamethyldisilazide environments between 0.16–0.36 ppm indicative of Mg-C/Si-H σ-bond metathesis as well as a new signal at 3.66 ppm which corresponded to a single proton by integration.

Preparative scale repetition of this reaction in toluene yielded crystals of compound **4**, a heterobimetallic hydride of the formula $[K\{N(SiMe_3)_2\}_2MgH]_2$, suitable for single crystal X-ray diffraction analysis, the results of which are shown in Fig. 2.6. Although this species is structurally analogous to the previously reported hydride, **V**, its synthesis is, as hoped, the result of selective Mg-C/Si-H σ-bond metathesis of the more reactive and less sterically encumbered alkyl group of compound **3**. The bond length and angle data of **4** are also similar to those observed for the analogous di-*iso*-propylamide analogue **V** with some notable elongation of bonds as a consequence of the more sterically encumbered hexamethyldisilazide ligands. The previously unattributed peak at 3.66 ppm in the ^{1}H NMR spectrum of **4** also corresponded to the chemical shift of the hydride peak of **V** and was, thus, assigned as the bridging hydride resonance. The persistence of the solid state structure in aromatic solvents was corroborated by the observation of a single diffusion coefficient in the ^{1}H DOSY NMR spectrum for both the hydride and silylmethyl signals, while no evidence for fluxional behaviour was observed in variable temperature experiments.

In contrast to this straightforward behaviour, an analogous reaction of **2** with phenylsilane in d_8-toluene provided a considerably more complex ^{1}H NMR spectrum with two notable peaks at 4.44 and 5.12 ppm attributed to the hydride resonances of $PhSi(H)_2n$-Bu and $PhSi(H)_2N(SiMe_3)_2$ respectively. This latter observation is suggestive of not only Mg-C/Si-H but also M-N/Si-H σ-bond metathesis. Also notable were the complex signals associated with the metal-bound–$N(SiMe_3)_2$ region, which consisted of overlapping peaks between 0.32

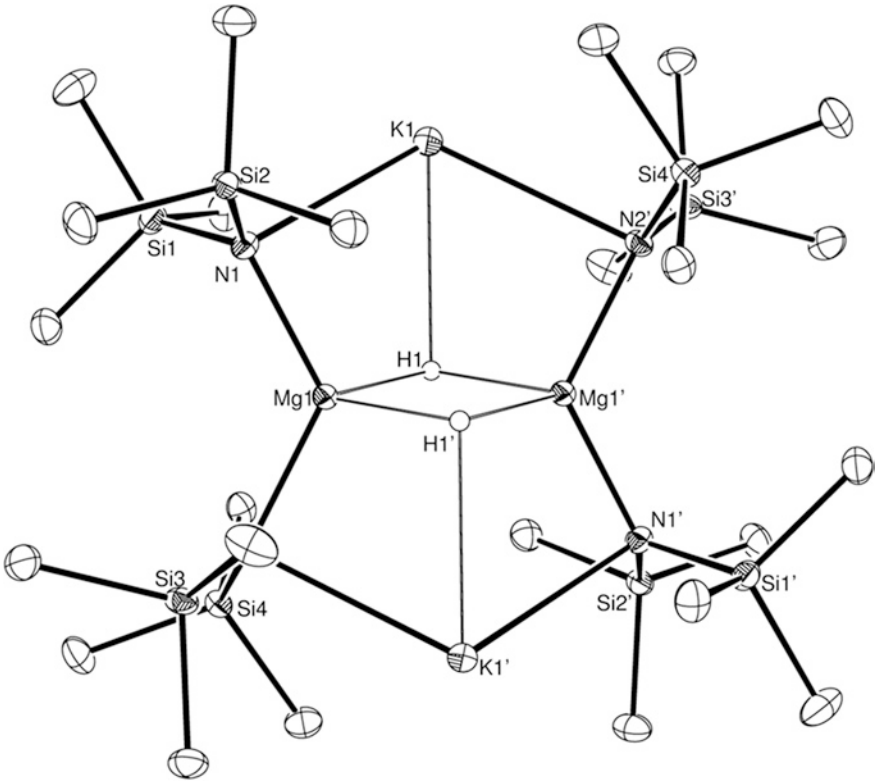

Fig. 2.6 ORTEP plot of **4** (30 % probability ellipsoids). H atoms apart from metal-bound hydrides omitted for clarity. Selected bond lengths (Å) and angles (°): Mg1-N1 2.0742(13), K1′-N2 2.9283(13), Mg1-H1 1.89(2), K1-H1 2.86(2), N1-Mg1-N2 124.97(5), N1-K1-N2′ 113.50(4), Mg1-H1-Mg1′ 106(1). Symmetry transformations used to generate equivalent atoms: x-1/2,-y + 1/2,z + 1/2, -x,-y + 1,-z + 1

and 0.47 ppm alongside a pair of broad overlapping signals centred on 3.87 and 3.69 ppm which integrated in a 144:4:6 ratio. In order to elucidate the origin of these observations, a preparative scale reaction undertaken in toluene provided compound **5**, a heterobimetallic hydride of the form $[Na_6Mg_6\{N(SiMe_3)_2\}_8H_{10}]$, as crystals suitable for X-ray crystallographic analysis. The results of this analysis are shown in Fig. 2.7.

Compound **5** is a heterododecametallic species ligated by eight hexamethyldisilazide and ten hydride ligands with a formula of $[Mg_6Na_6\{N(SiMe_3)_2\}_8H_{10}]$. Its formation and the side-product peaks observed in the in situ ^{1}H NMR experiments are rationalised by the stoichiometry shown in Eq. 1. Indeed, a repeat of the in situ NMR scale experiment with this stoichiometry yielded a stoichiometric quantity of compound **5**.

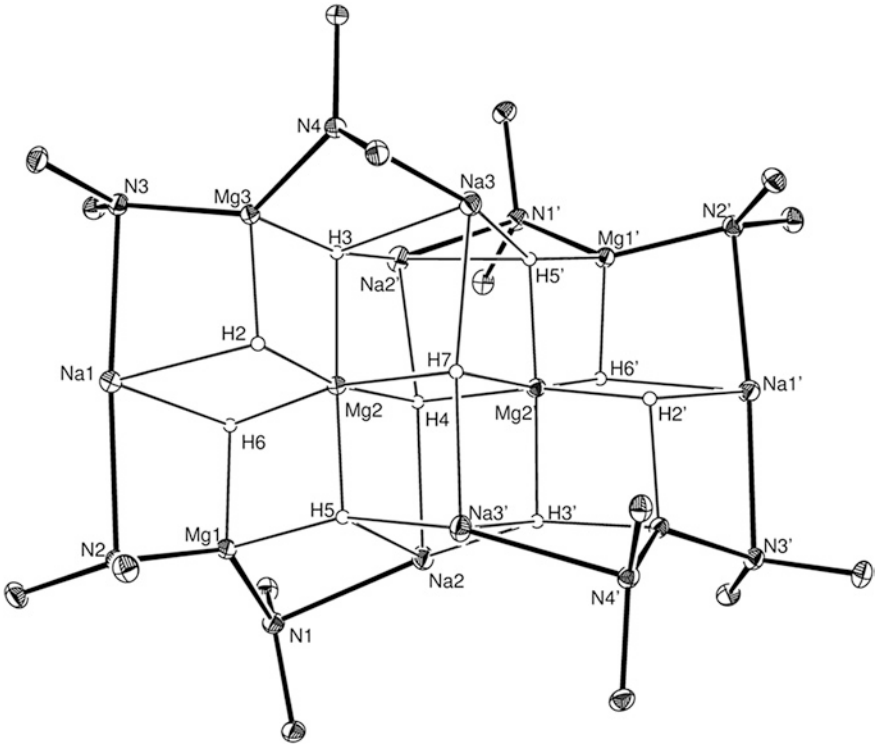

Fig. 2.7 ORTEP plot of **5** (30 % probability ellipsoids). H atoms apart from metal-bound hydrides and carbon atoms omitted for clarity. Selected bond lengths (Å) and angles (°): Na1-N2 2.6093(17), Na1-H2 2.34(2), Mg1-N2 2.0627(16), Mg2-H2 1.89(2), Mg2-H3 2.01(2), Mg2-H4 2.01(2), Na2-N1 2.5169(17), Na2-H4 2.385(7), Na2-H5 2.46(2), Mg1-N1 2.0534(16), Mg1-N2 2.0627(16), Mg2-H2-Na1 104(1), N2-Na1-N3 175.72(6), Mg2-H7-Mg2′ 103(1). Symmetry transformations used to generate equivalent atoms: -x + 2,y,-z + 3/2

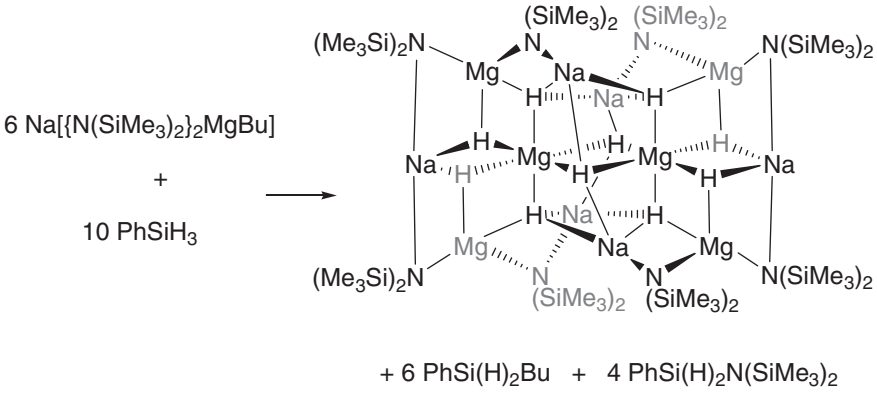

Equation 1 The proposed stoichiometry necessary to achieve compound **5**.

The formation of **5** constitutes a synthetic route which, although evidently selective for a specific compound, is not discriminating for the less bulky and more nucleophilic alkyl substituent over the present hexamethyldisilazides. Given the observed solution equilibria to which **2** appears to be subject it is therefore reasonable to speculate that the selective formation of **5** is in fact more a reflection of these equilibria than of the reactivity of substituents around the crystallographically defined structure of **2**.

The structure of **5** possesses a C_2 symmetry element running through the 2 central hydrides (H4 and H7), which bridge between two 6-coordinate magnesium centres (Mg2, Mg2′) ligated only by hydrides in a structural core reminiscent of magnesium dihydride. Perhaps imposed by the imperfect octahedral geometry of its $[Mg_2H_{10}]$ core, the Mg–H bonds of **5** are elongated in comparison to those observed in bulk MgH_2 (1.718 Å) [1]. The remaining four magnesium centres (Mg1, Mg3, Mg1′ and Mg3′) exist in identical coordination environments wherein the presence of two bulky hexamethyldisilazide ligands lowers their coordination number to four, with the other two sites occupied by hydrides bridging to the $[Mg_2H_{10}]$ core. The terminal sites of the potentially polymeric $[Mg_2H_{10}]$ core are capped by sodium atoms, Na1 and Na1′, which exist in a sawhorse conformation ligated axially by two amides. These ligands bridge to the tetracoordinate magnesium ions while two of the equatorial sites share hydrides, H2, H6, H2′ and H6′, with the $[Mg_2H_{10}]$ core. The residual sodium atoms (Na2, Na3, Na2′ and Na3′) are located in distorted tetrahedral sites which bridge, via hydrides H3, H5, H3′ and H5′, the central magnesium ions and are capped by amides shared with the tetracoordinate magnesium centres. These latter sodium ions form the vertices of cubic $[(NaMgH_2)_2]^{2+}$ clusters reminiscent of those observed by Stasch for the $[(LiH)_4]$ core of the structurally characterised lithium hydride, $[\{(DippNPPh_2)Li\}_4(LiH)_4]$ [14].

DOSY experiments (Fig. 2.8) performed on a crude sample of **5** suggested a single diffusion coefficient for the silylmethyl and hydride regions, corroborating the proposed peak attributions and suggesting that the solid state structure is retained in aromatic solvents (Table 2.4).

Although the crystallographically defined structure is suggestive of three hydride environments in a 2:4:4 ratio and two hexamethyldisilazide environments in a 1:1 ratio, the ^{1}H NMR spectrum at room temperature comprised only 2 broad, complex signals in a 4:6 ratio for the hydrides and a series of overlapping, second order peaks in the silylmethyl region. The more downfield hydride shift is suggested to be the 3-coordinate hydrides H2 and H6, with the six remaining, 4-coordinate hydrides providing the upfield signal at 3.87 ppm (Fig. 2.9).

Cooling the sample evidenced a fluxional process as a result of exchange of the tetracoordinate hydrides within the $[Mg_2H_{10}]$ core. At 267 K (calibrated utilising 4 % MeOH in MeOD) the 6H peak at 3.69 ppm was observed to split yielding two broad singlet resonances in a 2:4 ratio at 3.68 (H_a) and 3.59 ppm (H_b) respectively and a free energy of activation ($\Delta G^{\ddagger}$) for this process of 56 kJ mol^{-1} (Fig. 2.10).

The silylmethyl region at 248 K was split into two doublets at 0.32 and 0.48 ppm which can be attributed to the two observed hexamethyldisilazide environments each further split by the diastereotopic disposition imposed by the

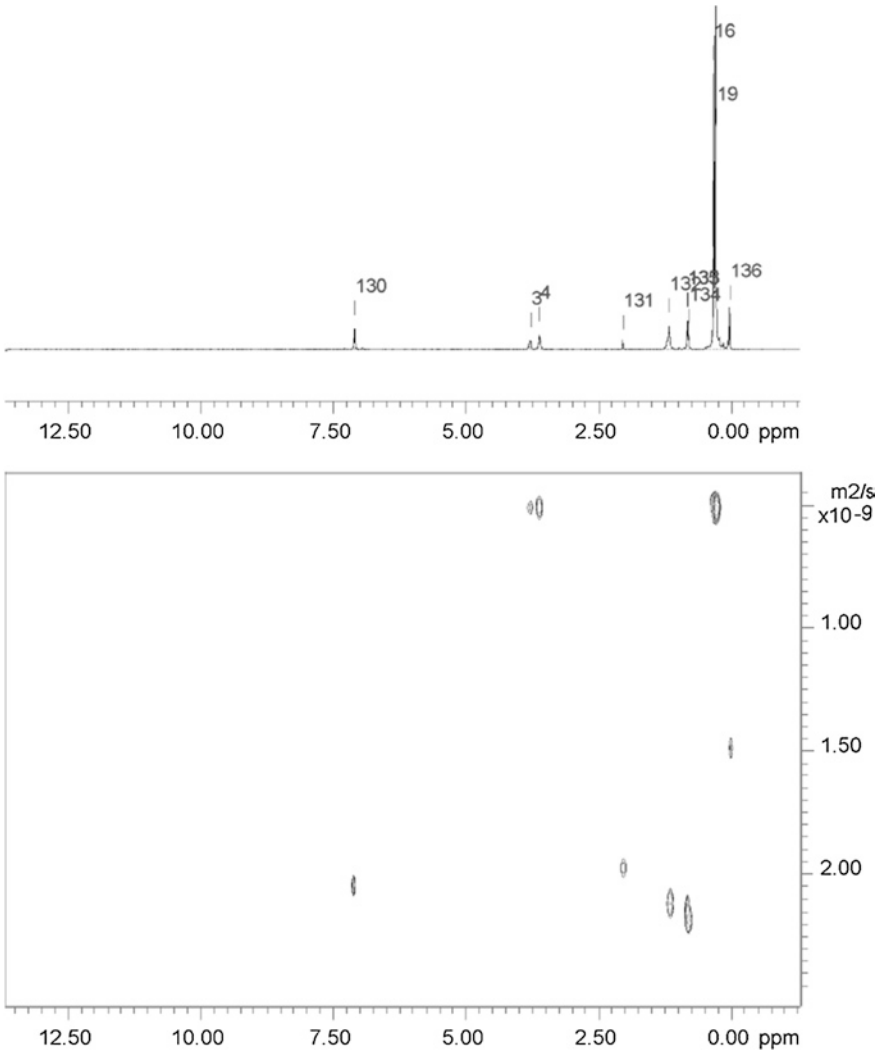

Fig. 2.8 The ^{1}H NMR and DOSY plots for a crude sample of compound **5**

rigidity of the cage structure. No coalescence temperature for the exchange of each separate hexamethyldisilazide environment, however, could be attained, even to the boiling point of the d_8-toluene solvent.

Attempts to extend this reactivity to the lightest congeneric analogue, **1**, yielded immediate precipitation of a fine, insoluble, colourless solid, thought to be various metal hydrides. NMR analysis suggested consumption of the $PhSiH_3$ and formation of $PhSi(H)_2Bu$ and $PhSi(H)_2N(SiMe_3)_2$ as well as silanes with higher alkyl and amide incorporation indicative of Mg-C/Si-H and Mg-N/Si-H σ-bond metathesis respectively. Repetition of this reaction in the more coordinating

Table 2.4 The diffusion coefficients, with relevant errors for the component ^{1}H NMR peaks of compound **5** as measured by DOSY

Proton	Peak	Chemical shift/ppm	Diffusion coefficient/m^2 s^{-1}	Error
Mg-H	3	3.781	5.27×10^{-10}	8.901×10^{-12}
Mg-H	4	3.610	5.29×10^{-10}	4.992×10^{-12}
(N(SiMe$_3$)$_2$)	16	0.328	5.26×10^{-10}	5.310×10^{-12}
(N(SiMe$_3$)$_2$)	17	0.301	5.29×10^{-10}	5.088×10^{-12}
(N(SiMe$_3$)$_2$)	18	0.292	5.31×10^{-10}	3.582×10^{-12}
(N(SiMe$_3$)$_2$)	19	0.284	5.29×10^{-10}	5.153×10^{-12}

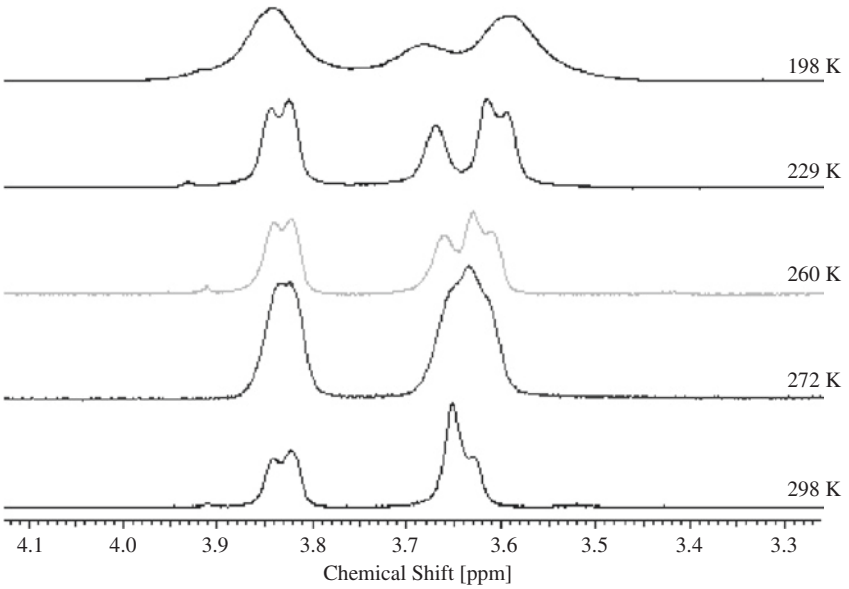

Fig. 2.9 The hydride region of the ^{1}H NMR of **5** below, at and above the coalescence temperature (uncalibrated temperatures)

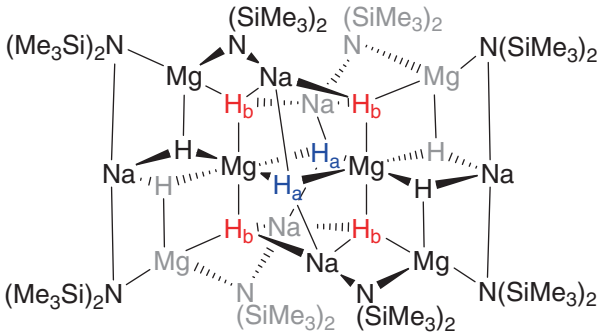

Fig. 2.10 The proposed fluxional hydrides (H_a and H_b) in complex **5**

solvent THF yielded an identical result, suggesting that extension to complex s-block polyhydrides of the lightest alkali metal is not possible with a hexamethyldisilazide co-ligand set under these conditions.

This chapter describes a novel series of s-block mixed metal amidoalkyls encapsulating a range of alkali metal cations with magnesium. These species show fascinating structural variation contingent on the identity of the Group 1 cation and resultant intermolecular interactions both in the solid state and solution. Further explored is the formation of heterobimetallic magnesium-alkali metal hydride clusters may be prepared by a σ-bond metathesis route from the corresponding s-block amidoalkyls bearing only simple ligands of catalytic relevance. While the formation of compound **4** suggests selective metathesis at the more reactive alkyl substituent, the formation of **5** requires less discriminative metathesis of both alkyl and amide ligands of **2**, and may, alongside the inaccessibility of a lithium analogue, represent a reflection of the solution equilibria which **1**–**3** are subject to. Nevertheless, this chapter indicates the under-represented utility of heteroleptic s-block clusters for metathesis chemistry and a novel approach to higher metal hydride clusters wherein the coordinative flexibility of a mixture of s-block elements allows them to act as both corner and edge occupying species. Work to extend this reactivity to the lightest alkali metal ion is ongoing, alongside studies into the reactivity of these novel and structurally interesting s-block species.

2.4 Experimental Data

[Li{N(SiMe$_3$)}$_2$MgBu], 1

To a toluene solution (2 mL) of di-*n*-butylmagnesium in heptanes (1 mmol, 2 mL) was added hexamethyldisilazane (1 mmol, 0.210 mL). The resultant solution bubbled and was stirred overnight after which time lithium hexamethyldisilazide (1 mmol, 167 mg) was added. Stirring was continued for 1 hour and the resultant suspension filtered, the solution was then used as is. Material suitable for crystallographic characterisation was procured by reducing this solution in vacuo to incipient crystallisation then cooling to −18 °C (265 mg, 67 %).

^{1}H NMR (300 MHz, d$_8$-Tol) δ ppm 0.01 (m, 2 H, MgC$\underline{H}_2$CH$_2$CH$_2$CH$_3$) 0.17 (s, 36 H, N(Si$\underline{Me}_3$)$_2$) 1.15 (t, 3 H, MgCH$_2$CH$_2$CH$_2$C$\underline{H}_3$) 1.64 (m, 2 H, MgCH$_2$C$\underline{H}_2$CH$_2$CH$_3$) 1.90 (m, 2 H, MgCH$_2$CH$_2$C$\underline{H}_2$CH$_3$). ^{13}C NMR (75 MHz, d$_8$-Tol) δ ppm 5.1 (N(Si$\underline{Me}_3$)$_2$), 11.2 (MgC$\underline{H}_2$CH$_2$CH$_2$CH$_3$) 14.4 (MgCH$_2$CH$_2$CH$_2$C$\underline{H}_3$) 31.8 (MgCH$_2$C$\underline{H}_2$CH$_2$CH$_3$) 32.5 (MgCH$_2$CH$_2$C$\underline{H}_2$CH$_3$).

In spite of repeated attempts, no consistent elemental analysis data could be obtained.

[Na{N(SiMe$_3$)}$_2$MgBu], 2

To a toluene solution (2 mL) of di-*n*-butylmagnesium in heptanes (1 mmol, 2 mL) was added hexamethyldisilazane (1 mmol, 0.210 mL). The resultant solution bubbled and was stirred overnight after which time sodium hexamethyldisilazide (1 mmol, 183 mg) was added. Stirring was continued for 1 h and the resultant suspension filtered, the solution was then used as is. Material suitable for crystallographic characterisation was procured by reducing this solution *in vacuo* to incipient crystallisation then cooling to −18°C (218 mg, 53 %).

^{1}H NMR (400 MHz, d$_8$-Tol) δ ppm −0.07 (m, 2 H, MgC$\underline{H}_2$CH$_2$CH$_2$CH$_3$) 0.19 (s, 36 H, N(Si$\underline{Me}_3$)$_2$) 1.18 (t, 3 H, MgCH$_2$CH$_2$CH$_2$C$\underline{H}_3$) 1.68 (m, 2 H, MgCH$_2$C$\underline{H}_2$CH$_2$CH$_3$) 1.92 (m, 2 H, MgCH$_2$CH$_2$C$\underline{H}_2$CH$_3$). ^{13}C NMR (100 MHz, d$_8$-Tol) δ ppm 6.0 (N(Si$\underline{Me}_3$)$_2$), 12.1 (MgC$\underline{H}_2$CH$_2$CH$_2$CH$_3$) 14.5 (MgCH$_2$CH$_2$CH$_2$C$\underline{H}_3$) 32.0 (MgCH$_2$C$\underline{H}_2$CH$_2$CH$_3$) 33.0 (MgCH$_2$CH$_2$C$\underline{H}_2$CH$_3$).

In spite of repeated attempts, no consistent elemental analysis data could be obtained.

[K{N(SiMe$_3$)}$_2$MgBu], 3

To a toluene solution (2 mL) of di-*n*-butylmagnesium in heptanes (1 mmol, 2 mL) was added hexamethyldisilazane (1 mmol, 0.210 mL). The resultant solution bubbled and was stirred overnight after which time potassium hexamethyldisilazide (1 mmol, 199 mg) was added. Stirring was continued for 1 hour and the resultant suspension filtered, the solution was then used as is. Material suitable for crystallographic characterisation was procured by reducing this solution in vacuo to incipient crystallisation then cooling to –18 °C (303 mg, 71 %).

^{1}H NMR (300 MHz, d$_8$-Tol) δ ppm −0.40 (m, 2 H, MgC$\underline{H}_2$CH$_2$CH$_2$CH$_3$) 0.22 (s, 36 H, N(Si$\underline{Me}_3$)$_2$) 1.20 (t, 3 H, MgCH$_2$CH$_2$CH$_2$C$\underline{H}_3$) 1.67 (m, 2 H, MgCH$_2$C$\underline{H}_2$CH$_2$CH$_3$) 1.92 (m, 2 H, MgCH$_2$CH$_2$C$\underline{H}_2$CH$_3$). ^{13}C NMR (75 MHz, d$_8$-Tol) δ ppm 6.3 (N(Si$\underline{Me}_3$)$_2$), 14.0 (MgC$\underline{H}_2$CH$_2$CH$_2$CH$_3$) 14.6 (MgCH$_2$CH$_2$CH$_2$C$\underline{H}_3$) 32.0 (MgCH$_2$C$\underline{H}_2$CH$_2$CH$_3$) 33.0 (MgCH$_2$CH$_2$C$\underline{H}_2$CH$_3$).

Anal. calc'd for $C_{15}H_{43}KMgN_2Si_4$ C, 42.17; H, 10.14; N, 6.56 %. Found C, 43.32; H, 10.15; N, 6.26 %.

[K{N(SiMe$_3$)$_2$}$_2$MgH]$_2$, 4

To a toluene solution (3 mL) of **2** (1 mmol in 4 mL 1:1 toluene:heptanes) was added phenylsilane (1 mmol, 0.123 mL) and the resultant solution stirred overnight. Subsequent filtration followed by concentration to incipient crystallisation and chilling to −35 °C yielded colourless blocks suitable for X-ray analysis (262 mg, 68 %).

^{1}H NMR (400 MHz, d$_8$-Tol) δ ppm 0.19–0.31 (m, 36 H, N(Si$\underline{Me}_3$)$_2$) 3.66 (s, 1 H, Mg-$\underline{H}$). ^{13}C NMR (75 MHz, d$_8$-Tol) δ ppm 6.1 (N(Si$\underline{Me}_3$)$_2$) 6.2 (N(Si$\underline{Me}_3$)$_2$) 6.8 (N(Si$\underline{Me}_3$)$_2$).

Anal. calc'd for $C_{24}H_{74}K_2Mg_2N_4Si_8.C_6H_5CH_3$: C, 43.17; H, 9.58; N, 6.50 %. Found: C, 42.81; H, 9.98; N, 6.17 %.

$[Na_6Mg_6\{N(SiMe_3)_2\}_8H_{10}]$, 5

To a toluene solution (3 mL) of **2** (1 mmol in 4 mL 1:1 toluene:heptanes) was added phenylsilane (1.66 mmol, 0.204 mL) and the resultant solution stirred overnight. Subsequent filtration followed by concentration to incipient crystallisation and chilling to −35 °C yielded colourless blocks suitable for X-ray analysis (139 mg, 53 %).

^{1}H NMR (400 MHz, d_8-Tol) δ ppm 0.28–0.48 (m, 144 H, N(Si<u>Me</u>$_3$)$_2$) 3.54–3.75 (m, 6 H, Mg-<u>H</u>), 3.75–3.93 (m, 4 H, Mg-<u>H</u>). ^{13}C NMR (100 MHz, d_8-Tol) δ ppm 7.0 (N(Si<u>Me</u>$_3$)$_2$), 7.3 (N(Si<u>Me</u>$_3$)$_2$), 7.4 (N(Si<u>Me</u>$_3$)$_2$).

Anal. calc'd for $C_{48}H_{154}Mg_6N_8Na_6Si_{16}$: C, 36.56; H, 9.84; N, 7.11 %. Found: C, 36.44; H, 9.68; N, 6.95 %.

M. p. 162–~200 °C (dec.)

	1	**2**	**3**	**4**	**5**
Empirical formula	$C_{16}H_{45}LiMgN_2Si_4$	$C_{16}H_{45}NaMgN_2Si_4$	$C_{16}H_{45}KMgN_2Si_4$	$C_{12}H_{37}KMgN_2Si_4$	$C_{27.50}H_{81}Mg_3N_4Na_3Si_8$
Formula weight (g mol^{-1})	409.15	425.20	441.31	385.21	834.58
Crystal system	Monoclinic	Monoclinic	Monoclinic	Monoclinic	Monoclinic
Space group	$P2_1/n$	$P2_1/n$	$P2_1/n$	$P2_1/n$	C_2/c
a (Å)	a = 9.2930(1) Å alpha = 90°	9.3020(2)	9.2520(2)	9.4600(1)	25.2680(2)
b (Å)	20.3790(4)	20.6500(4)	20.5140(4)	14.8070(2)	17.8740(2)
c (Å)	13.8580(3)	13.9670(3)	14.6960(3)	16.5070(3)	24.3340(3)
α (°)	90	90	90	90	90
β (°)	98.2550(10)	96.493(1)	93.112(1)	90.168(1)	104.234(1)
γ (°)	90	90	90	90	90
V (Å)	2597.26(8) Å^3	2665.66(10) Å^3	2785.12(10) Å^3	2312.20(6) Å^3	10652.8(2) Å^3
Z	4	4	4	4	8
ρ (g cm^{-3})	1.046 Mg/m^3	1.059 Mg/m^3	1.052 Mg/m^3	1.107 Mg/m^3	1.041 Mg/m^3
μ (mm^{-1})	0.255	0.266	0.389	0.459	0.283
θ range (°)	3.73–27.49	3.60–27.49	4.66–27.49	3.56–27.46	3.52–27.50
Measured/ independent reflections/R_{int}	30373/ 5873/ 0.0580	48709/ 6100/ 0.0746	45366/ 6345/ 0.0632	30880/ 5256/ 0.1116	73776/ 12160/ 0.0460
Data/ restraints/ parameters	5873/1/238	6100/0/230	6345/48/287	5256/0/197	12160/ 36/466

Goodness-of-fit on F^2	1.249	1.104	1.154	1.075	1.084
R_1, wR_2 [$I > 2\sigma(I)$]	0.0574, 0.1402	0.0480, 0.1026	0.1518, 0.4129	0.0362, 0.0942	0.0399, 0.1044
R_1, wR_2 (all data)	0.0673, 0.1446	0.0788, 0.1135	0.1637, 0.4190	0.0401, 0.0978	0.0550, 0.1141

Notes on crystal refinement

1 Mg1 and Li1 were seen to be closely disordered with each other in an 88:12 ratio. The minor disordered fractional occupancy atoms have been denoted with labels Mg1A and Li1A and they were treated isotropically in order to assist convergence. An additional distance restraint was also included, namely, to maintain a distance of 0.3 Å between Mg1 and Li1A. Unsurprisingly, the latter 12 % fractional-occupancy alkali metal benefited from the stability that this restraint imposed

3 Potassium, and *n*-butyl group based on C13 disordered over 2 sites in a 50:50 ratio. Some ADP restraints added in the disordered butyl group to assist convergence

4 Asymmetric unit comprises 1 potassium cation plus ½ of a dimer anion. The latter straddles a crystallographic inversion centre which serves to generate the remainder of this species. The hydride (H1) was located and refined without restraints

5 The asymmetric unit comprises half of a molecule and a toluene solvent entity with half site occupancy. The remainder of the former is generated via a 2-fold rotation axis implicit in the space group symmetry. The solvent moiety also straddles this rotation axis and, as such is disordered about same in the gross structure. In addition, the methyl group could not be reliably located in the solvent, which probably reflects positional disorder between the 6 ring carbon positions. In effect, the solvent was treated as a benzene in the refinement, with account of the missing, half-occupancy solvent methyl group is accounted for in the formula herein. The phenyl ring was treated as a regular hexagon during refinement, and the ADPs therein were restrained to assist convergence

References

1. R.E. Mulvey, Acc. Chem. Res. **42**, 743 (2009); R.E. Mulvey, Dalton Trans. **42**, 6676 (2013)
2. L.T. Wendell, J. Bender, X. He, B.C. Noll, K.W. Henderson, Organometallics **25**, 4953 (2006)
3. A.J. Martinez-Martinez, D.R. Armstrong, B. Conway, B.J. Fleming, J. Klett, A.R. Kennedy, R.E. Mulvey, S.D. Robertson, C.T. O'Hara, Chem. Sci. **5**, 771 (2014)
4. F. Ortu, G.J. Moxey, A.J. Blake, W. Lewis, D.L. Kays, Inorg. Chem. **52**, 12429 (2013)
5. S. Aldridge, A.J. Downs, Chem. Rev. **101**, 3305 (2001)
6. F. Buch, H. Brettar, S. Harder, Angew. Chem.-Int. Ed. **45**, 2741 (2006); F. Buch, S. Harder, Organometallics **26**, 5132 (2007); Z. Naturforsch., B: Chem. Sci. **63**, 169 (2008); M. Arrowsmith, M.S. Hill, T. Hadlington, G. Kociok-Köhn, C. Weetman, Organometallics **30**, 5556 (2011); M. Arrowsmith, T.J. Hadlington, M.S. Hill, G. Kociok-Köhn, Chem. Commun. **48**, 4567 (2012)
7. J.F. Dunne, S.R. Neal, J. Engelkemier, A. Ellern, A.D. Sadow, J. Am. Chem. Soc. **133**, 16782 (2011); M.S. Hill, D.J. Liptrot, D.J. MacDougall, M.F. Mahon, T.P. Robinson, Chem. Sci. **4**, 4212 (2013)
8. M.S. Hill, M.F. Mahon, T.P. Robinson, Chem. Commun. **46**, 2498 (2010)
9. A.G.M. Barrett, M.R. Crimmin, M.S. Hill, P.B. Hitchcock, P.A. Procopiou, Organometallics **26**, 4076 (2007); D.J. Liptrot, M.S. Hill, M.F. Mahon, D.J. MacDougall, Chem. Eur. J. **16**, 8508 (2010)
10. M. Kelly, in *Fuel Cells and Hydrogen Storage*, vol. 141, eds. by A. Bocarsly, D. M. P. Mingos (Springer, Berlin Heidelberg, 2011)

11. F. Schuth, B. Bogdanovic, M. Felderhoff, Chem. Commun. **20,** 2249 (2004); M. Dornheim, S. Doppiu, G. Barkhordarian, U. Boesenberg, T. Klassen, O. Gutfleisch, R. Bormann, Scripta Materialia **56**, 841 (2007); K.-F. Aguey-Zinsou, J.-R. Ares-Fernandez, Energy Environ. Sci. **3**, 526 (2010); I.P. Jain, C. Lal, A. Jain, Int. J. Hydrogen Energy **35**, 5133 (2010)
12. S. Harder, Chem. Commun. **48**, 11165 (2012); R.W.P. Wagemans, J.H. van Lenthe, P.E. de Jongh, A.J. van Dillen, K.P. de Jong, J. Am. Chem. Soc. **127**, 16675 (2005)
13. M. Arrowsmith, M. S. Hill, D.J. MacDougall, M.F. Mahon, Angew. Chem.-Int. Ed. **48**, 4013 (2009)
14. Harder, J. Spielmann, J. Intemann, H. Bandmann, Angew. Chem.-Int. Ed. **50**, 4156 (2011)
15. J. Intemann, J. Spielmann, P. Sirsch, S. Harder, Chem.- Eur. J. **19**, 8478 (2013)
16. Hoffmann, T. Kottke, R.J. Lagow, R.D. Thomas, Angew. Chem.-Int. Ed. **37**, 1537 (1998)
17. A. Stasch, Angew. Chem.-Int. Ed. **51**, 1930 (2012)
18. A. Stasch, Angew. Chem.-Int. Ed. **53**, 1338 (2014)
19. D.J. Gallagher, K.W. Henderson, A.R. Kennedy, C.T. O'Hara, R.E. Mulvey, R.B. Rowlings, Chem. Commun. 376 (2002); D.V. Graham, A.R. Kennedy, R. E. Mulvey, C.T. O'Hara, Acta Crystallogr. Sect. C **62**, m366 (2006)
20. P.C. Andrikopoulos, D.R. Armstrong, A.R. Kennedy, R.E. Mulvey, C.T. O'Hara, R.B. Rowlings, Eur. J. Inorg. Chem. **2003**, 3354 (2003)
21. A. Streitwieser, Acc. Chem. Res. **17**, 353 (1984); R. Benn, A. Rufińska, Angew. Chem.-Int. Ed. **25**, 861 (1986); N.N. Greenwood, A. Earnshaw, *Chemistry of the Elements*, 2nd edn. (Elsevier, New York, 1997), pp. 102–105, 127
22. J. Francos, B.J. Fleming, P. Garcia-Alvarez, A.R. Kennedy, K. Reilly, G.M. Robertson, S.D. Robertson, C.T. O'Hara, Dalton Trans. **43**, 14424 (2014)

http://www.springer.com/978-3-319-21035-3

Group 2 Mediated Dehydrocoupling
Liptrot, D.J.
2016, XV, 162 p. 169 illus., 3 illus. in color., Hardcover
ISBN: 978-3-319-21035-3